Understanding the high-resolution spectral signature of the $\mathrm{N_2-H_2O}$ van der Waals complex in the $2\mathrm{OH}$ stretch region

R. Glorieux,[1] B. M. Hays,[1] A. S. Bogomolov,[2] M. Herman,[3] T. Vanfleteren,[3] N. Moazzen-Ahmadi,[4] and C. Lauzin[1]

[1)] *Institute of Condensed Matter and Nanosciences, Université catholique de Louvain (UCLouvain), Chemin du cyclotron, 2 1348 Louvain-la-Neuve, Belgium.*

[2)] *Voevodsky Institute of Chemical Kinetics and Combustion, Institutskaya Str. 3, Novosibirsk, Russia.*

[3)] *Spectroscopy, Quantum Chemistry and Atmospheric Remote Sensing (SQUARES), Faculté des Sciences, Université libre de Bruxelles (ULB), 50 ave. F-D Roosevelt, B-1050, Brussels, Belgium.*

[4)] *Department of Physics and Astronomy, University of Calgary, 2500 University Drive North West, Calagry, Alberta T2N 1N4, Canada.*

(Dated: 28 April 2023)

We present the observation of the $\mathrm{N_2-H_2O}$ van der Waals complex in the $2\mathrm{OH}$ stretch overtone region. The high-resolution jet cooled spectra were measured using a sensitive continuous-wave cavity ringdown spectrometer. Several bands were observed and vibrationally assigned in terms of v_1, v_2 and v_3, the vibrational quantum numbers of the isolated $\mathrm{H_2O}$ molecule, as $(v_1'v_2'v_3') \leftarrow (v_1''v_2''v_3'') = (200) \leftarrow (000)$ and $(101) \leftarrow (000)$. A combination band involving the excitation of the in-plane bending motion of $\mathrm{N_2}$ and the (101) vibration of water is also reported. The spectra were analysed using a set of four asymmetric top rotors, each associated with a nuclear spin isomer. Several local perturbations of the (101) vibrational state were observed. These perturbations were assigned to the presence of the nearby (200) vibrational state and to the combination of (200) with intermolecular modes.

I. INTRODUCTION

The $\mathrm{N_2-H_2O}$ van der Waals complex is composed of the most abundant constituent of Earth's atmosphere ($\mathrm{N_2}$) and of the most important greenhouse gas ($\mathrm{H_2O}$). The equilibrium constant of formation of the $\mathrm{N_2-H_2O}$ complex from $\mathrm{N_2}$ and $\mathrm{H_2O}$ was calculated using *ab initio* methods and statistical mechanics.[1] Its abundance was then evaluated in the Earth's atmosphere to be on the order of 10^{-2} mbar near the surface.[1] The calculated partial pressure of this complex is significant and comparable to that for $\mathrm{CO_2}$ near the surface. This value could be considered as an upper bound limit because of the assumptions made in this evaluation and comparison with other high-level calculations on similar complexes, i.e. $\mathrm{O_2-H_2O}$[2] also studied in Ref. 1.

A large amount of theoretical works on the $\mathrm{N_2-H_2O}$ complex have been reported. Directly relevant to this work, there is a high-level intermolecular potential energy surface (PES) by Tulegenov *et al.* [3]. This PES was later used by Wang and Carrington Jr. to solve the nuclear Hamiltonian and predict the (intermolecular) rovibrational levels.[4] Recently the bending (Q_2) intramolecular coordinate of water was explicitly included in the construction of the PES and in the calculation of rovibrational states.[5] This was performed by averaging the PES over the vibrational eigenfunction of the one dimensional Q_2 problem. In these two works, the intermolecular vibrational frequencies were predicted at a high level of precision but without assignment of the vibrational modes and information on the intensities of the associated transitions. In the rest of this manuscript, the predicted intermolecular modes of these studies will be numbered as a function of energy for a given K_a value. Sadlej *et al.* [6] and Ellington and Tschumper [7] also predicted the vibrational frequencies and additionally, the relative magnitude of the oscillator strength of the intermolecular modes and fundamental vibrations, but with a lower level of accuracy. In the work by Ellington and Tschumper [7], electronic structure calculations were performed using the CCSD(T) method and up to haQZ basis set. Information provided in these two works allow to assign partly the intermolecular modes in terms of relative motions of the $\mathrm{H_2O}$ and $\mathrm{N_2}$ units. The fundamental and overtone intramolecular OH-stretching frequencies and intensities of $\mathrm{N_2-H_2O}$ amongst other complexes were also calculated by Kjaergaard *et al.* [8].

Experimentally, the $\mathrm{N_2}$−water complex was first studied in the microwave region by Leung and collaborators[9] and subsequently by Stockman,[10] who extended the measurements in the millimeter-wave region. Here the spectra showed clear splitting of each rotational line. The study of the different isotopologues of this complex allowed to rationalize this splitting in terms of tunneling dynamics between the four equivalent minima of the PES of the complex. The spectra were assigned using the G_8 permutation inversion symmetry group. Later on, the $\mathrm{N_2-H_2O}$ complex was studied in the mid-infrared. The observed band was vibrationally assigned to the intramolecular bend excitation $(010) \leftarrow (000)$ of $\mathrm{H_2O}$ within $\mathrm{N_2-H_2O}$. The same G_8 symmetry group was used in addition to a Hamiltonian that takes into account explicitly one (of the two) tunneling coordinates.[11] Recently, $\mathrm{N_2-D_2O}$ was studied in the fundamental OD stretch region by some of the authors of this study.[12] Other experimental studies include lower resolution infrared investigations of $\mathrm{N_2-H_2O}$ embedded in rare gas matrices[13–17] and helium nanodroplets.[18]

In this work we report the first observation of this complex in the $2\mathrm{OH}$ stretch overtone region. Section II presents the experimental methodology that allowed us to observe the spectra. In Sec. III, we detail the vibrational and line by line rotational assignments with the aid of group theory. The Sec. IV presents the main effect of this extreme excitation, up to 29 times the dissociation energy, on the intra and intermolecular dynamics. Concluding remarks are given in Sec. V.

II. EXPERIMENTAL

The spectra were recorded at UCLouvain using the Continuous Wave Cavity Ring Down Spectrometer (CW-CRDS) and a pulsed slit supersonic expansion, both implemented in the FANTASIO+ (for "Fourier trANsform, Tunable diode and quAdrupole masS spectrometers Interfaced to a supersOnic expansion") set-up, originally set up in ULB. This instrument is described in previous publications.[19,20] Briefly, $N_2 - H_2O$ was formed from the expansion through a pulsed slit valve of a mixture of N_2 and He bubbling in distilled water.[20] The length and width of the slit are $l = 3$ cm and approximately 80 µm, respectively. The valve typically operates at 2 Hz with 25 ms pulse duration. Under these conditions, the backing pressure was around 8 bar and the residual pressure of the chamber was 7×10^{-3} mbar. The optical cavity of the CRDS spectrometer is composed of two concave mirrors (Layertech 154209, radius = 1000mm, reflectivity ≈ 99.999%) mounted on the vacuum chamber. The length separating the two mirrors is now $L \sim 75$ cm. The ring-down time of the empty cavity was typically equal to $\tau_0 = 120$ µs. In order to perform pulsed jet measurements, the ring downs were sorted as described in Ref. 20, with ON/OFF ring downs measured in between 4/170 and 20/370 ms after the TTL rise associated to the opening of the valve. Between 100 and 200 ring downs were fitted per spectral point, depending on the measured bands. The subtraction of the mean of the ring downs measured when the valve is OPEN/CLOSE gives directly access to the absorption coefficient α, expressed as:

$$\alpha = \left(\frac{1}{\tau} - \frac{1}{\tau_0}\right)\frac{L}{cl}, \tag{1}$$

where τ (τ_0) is the mean characteristic decay time with (without) gas and c is the speed of light in vacuum. Line positions were calibrated to $\pm 1 \times 10^{-3}$ cm^{-1} using spectral lines of hot (from the empty vacuum chamber) and cold (from the supersonic jet expansion) water monomer lines position with wavenumbers retrieved from HITRAN.[21] Following the relative intensities of the rotational structure in the observed bands, the rotational temperature of the complex was found to be around 15 K. Four DFB laser diodes (NTT Electronics, centered at 1375, 1380 and 1384 nm; 10 mW, 1 MHz linewidth and Eblana Photonics, centered at 1388 nm; 10 mW, 1 MHz linewidth) coupled to a booster optical amplifier (Thorlabs BOA1410S) were used in this work.

III. SPECTRAL ASSIGNMENT AND ANALYSIS

The equilibrium geometry of $N_2 - H_2O$ is planar with the N_2 molecule nearly colinear with the $O - H$ bond.[4,6] This complex is an asymmetric top characterized by the total angular momentum J and its projection on the a and c inertial axis, labeled K_a and K_c, respectively. The potential energy surface of the complex contains four equivalent minima. Using Bunker and Jensen[22] notations, we will call them the different versions of the complex hereafter and label them V_1, V_2, V_3 and V_4 as illustrated in Fig. 1. The lowest energy paths between the different versions are an internal rotation of the water molecule (corresponding to the molecular symmetry group operation (12) connecting V_1 to V_3 or V_2 to V_4) and a concerted motion of the two subunits of the complex[4,5,9,11] (corresponding to the (12)(34) operation connecting V_1 to V_2 or V_3 to V_4). This will be noted $N - N$ tunneling hereafter. Due to these internal dynamics, each rotational energy level of the complex is split in four levels.

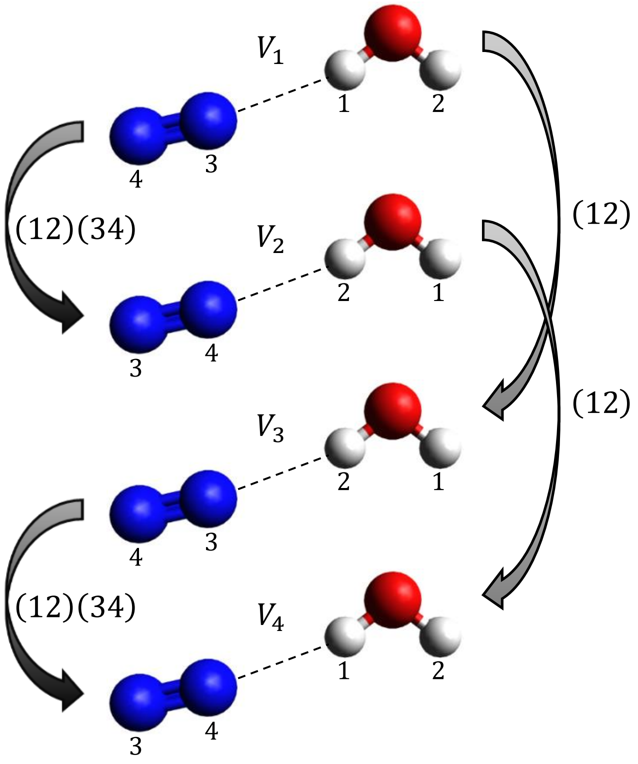

FIG. 1. Representation of the four equivalent minima of the potential energy surface of the $N_2 - H_2O$ complex, labeled as V_1, V_2, V_3 and V_4. The H nuclei in white are labeled 1 and 2 and the N nuclei in blue 3 and 4. Indicated operations are associated with the molecular symmetry group operation exchanging equivalent nuclei and connecting the different versions of the complex.

The labeling of the energy levels is made in terms of the irreducible representations of the molecular symmetry group of the complex G_8. The character table associated with this group can be found in Table VIII in the work by Coudert and Hougen.[23] By considering the different degrees of freedom of the complex as decoupled, the irreducible representations of the tunneling wavefunction are A_1^+, A_2^+, B_1^+ and B_2^+. The symmetry of the Vibration-Rotation-Tunneling (VRT) energy levels are $A_1^\pm$, $A_2^\pm$, $B_1^\pm$ and $B_2^\pm$ where the superscript ± refers to the symmetry of the state under the inversion operation E^*: + (−) indicates that the state is symmetric (anti-symmetric) under E^*. The ± superscript can also be related to the parity of the K_c quantum number because the irreducible representation of the rotational wavefunction is A_1^+ if K_aK_c are respectively *even even* or *odd even* and A_1^- if K_aK_c are respectively *even odd* or *odd odd*. The label A (B) indicates that a state is symmetric (anti-symmetric) with respect to the permutation operation (12) (water tunneling motion). As the irreducible representation of the electric dipole moment is A_1^-, the selection rule is $+ \leftrightarrow -$ for each tunneling state. To simplify the notations, the superscript $+/-$ will not be used in the remainder of this manuscript. Each VRT state will thus be referred to as A_1, A_2, B_1 or B_2. The relative nuclear spin statistical weight of the VRT states are 2, 1, 6 and 3, respectively. Since the splitting associated to the $\mathrm{N-N}$ tunneling motion was not observed for most of the measured bands, we will call the combination of each "pair" of states A (contribution of A_1 and A_2) and B (contribution of B_1 and B_2) states. Their nuclear spin statistical weight will then be 3 and 9, respectively.

Vibrational assignment

The spectra recorded in the 2OH stretch region are presented in Fig. 2 with the associated vibrational and $K_a' \leftarrow K_a''$ assignments. In this figure, the vertical dashed lines represent the $(200) \leftarrow (000)$ and $(101) \leftarrow (000)$ band origins of the isolated $\mathrm{H_2O}$. The other nearby vibrational states[24,25] of $\mathrm{H_2O}$ corresponding to (021) and (002) are more than 300 $\mathrm{cm^{-1}}$ below and nearly 200 $\mathrm{cm^{-1}}$ above the energy range of Fig. 2, respectively. The vibrational assignments of the $(200) \leftarrow (000)$ and $(101) \leftarrow (000)$ a-type $K_a' \leftarrow K_a'' = 0 \leftarrow 0$ subbands were thus straightforward due to the proximity of the subbands with the vibrational band origin of the monomer. The assignment of the associated b-type subbands in Fig. 2 was based on previous experimental studies of the complex[10,11] and the value of the A rotational constant retrieved in these studies. The observation of Q-branches also secured these assignments. The band around 7281 $\mathrm{cm^{-1}}$ was assigned to the combined excitation of the intermolecular in-plane $\mathrm{N_2}$ bending mode (ν_{int}) and of the intramolecular (101) vibration of $\mathrm{H_2O}$. This assignment is discussed in Sec. IV.

In Fig. 3, the energy level diagram of the $\mathrm{N_2-H_2O}$ complex in the ground (from Ref. 4) and in the excited vibrational states (200) (left panel) and (101) (right panel) from this work is illustrated. In this diagram, solid arrows represent a-type transitions and dashed arrows represent b-type transitions, while blue and red arrows represent the observed transitions arising from the different tunneling states A and B, respectively. The splitting associated with the water tunneling motion for a specific K_a value is noted as Δ_{K_a}. The character '$\sim$' indicates the splittings in the excited vibrational states. As the irreducible representations of the (100) and (001) vibrational wavefunctions of water in the complex are A_1^+ and B_1^+, respectively, we measure the difference in the tunneling splittings between the ground vibrational state and (200) whereas the sum of the tunneling splittings is observed for the $(101) \leftarrow (000)$ band.

Line by line analysis

A global fit was performed including all the transitions previously observed in the microwave,[9] millimeter-wave[10] and infrared (IR)[11] regions. These transitions were fitted with a weight proportional to their experimental uncertainties using the PGOPHER software.[26] Nuclear spin isomers (each associated to an unique tunneling state) were modeled using the S-reduced Watson asymmetric top Hamiltonian.[27] The vibrational states involved in this fit are the ground state from Refs. 9 and 10, the (010) state from Ref. 11 and the (200) and (101) states from this work. The refined ground state rotational constants from this global fit can be found in Table I and those for the (010) bending vibrational state are listed in Table S-1 of the supplementary materials. The reported transitions in the ground[9,10] and (010)[11] vibrational states included in the global fit are given in Table S-2 and S-3 of the supplementary materials.

The $(200) \leftarrow (000)$ *band*

As shown in Fig. 2, three subbands were observed for the $(200) \leftarrow (000)$ vibrational band, one a-type $K_a' \leftarrow K_a'' = 0 \leftarrow 0$ (and $1 \leftarrow 1$) and two b-type $K_a' \leftarrow K_a'' = 1 \leftarrow 0$ and $0 \leftarrow 1$. Top and bottom panels in Fig. 4 show the measured (in the top panel in blue) and simulated (in black) spectra for the b-type $K_a' \leftarrow K_a'' = 1 \leftarrow 0$ and a-type subbands, respectively. The two series of lines labeled A and B arise from the $\mathrm{H_2O}$ tunneling splitting. The analysis of the $K_a' \leftarrow K_a'' = 0 \leftarrow 0$ subband was straightforward due to the well behaved relative intensities between the two tunneling states that follow the expected nuclear spin statistical weight and a clear rotational progression. The $\mathrm{N-N}$ splitting, predicted in Ref. 4 to be on the order of 10^{-4} $\mathrm{cm^{-1}}$ was not observed for this subband as was the case for the a-type subband in the IR study in Ref. 11. Broad features on the low frequency side of the parallel band marked with a circle 'o' are due to the water dimer.[28] For the b-type subbands, the assignment of the most intense transitions was straightforward as there was no doubling of the transitions due to the $\mathrm{N-N}$ tunneling splitting. The Q-branch was congested precluding the assignment of some lines of the B_2 tunneling state. On the contrary, the signature of the tunneling motion is evident for the A states tunneling subbands, as illustrated in top panel of Fig. 4. The two series of lines arising from the A_1 and A_2 tunneling states are clearly resolved. The assignment of each subband was based on relative intensities determined from the nuclear spin statistical weight associated with each tunneling states. The assignment of the a-type $K_a' \leftarrow K_a'' = 1 \leftarrow 1$ subband was made after analysis of the other subbands which provided a more refined set of molecular parameters.

The assigned transitions and their wavenumber are provided in Table S-4 of the supplementary materials. The rotational constants of the $\mathrm{N_2-H_2O}$ complex for the (200) vibrational state are given in Table II.

Finally, for a more faithful simulation of the spectral sig-

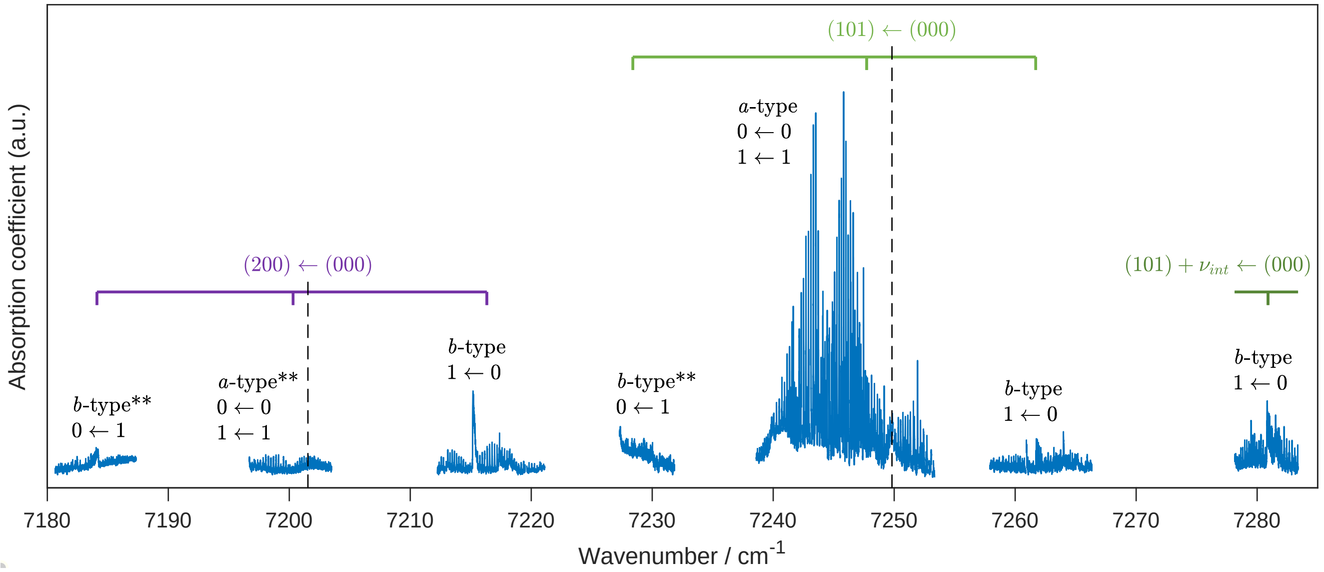

FIG. 2. Measured absorption spectra of $N_2 - H_2O$ in the 2OH stretch region. Vibrational bands are assigned following the isolated water vibrational quantum numbers. The dashed black vertical lines indicates the vibrational origins of isolated H_2O from Refs. 24 and 25. The $K_a' \leftarrow K_a''$ assignment of each subband is indicated below the subbands type. Due to small change in the experimental conditions, the relative intensities of the complex is uncertain by a factor up to 1.3. The intensity of the observed subbands marked with double asterisk '**' was multiplied by a factor two.

TABLE I. Refined $N_2 - H_2O$ ground vibrational state molecular constants (in cm^{-1}) [a] from the global fit.

	Ground vibrational state			
	A_1	A_2	B_1	B_2
A	18.108000(22)	18.062309(22)	15.981614(19)	15.989857(19)
B	0.0979503(27)	0.0977370(10)	0.0976869(11)	0.0977106(11)
C	0.0959790(27)	0.0961545(10)	0.0967240(11)	0.0967073(11)
$10^3 D_{JK}$	-2.8580(18)	-3.2020(18)	-2.0250(12)	-1.9689(13)
$10^6 D_J$	1.4518(88)	1.3857(60)	1.4209(89)	1.432(11)
$10^6 d_1$	-0.283(34)		-0.1544(78)	-0.1860(77)
$10^6 H_{JK}$	-0.560(37)	-1.452(32)	-0.950(19)	-0.794(20)
$10^9 H_J$	0.247(79)		0.120(32)	0.148(59)
$10^9 L_{JJK}$			0.433(63)	0.268(69)

[a] Numbers in parentheses are the uncertainties and are in the same units.

natures observed in the (200) region, we performed a Voigt line profile fit of 38 transitions while keeping the full width at half maximum (FWHM) of the Gaussian profile fixed at its Doppler value corresponding to 15 K, i.e. 0.003 cm^{-1}. This value was determined from the relative intensities of assigned rovibrational transitions and assuming an equilibrium between translation and rotation degrees of freedom. A mean value of the Lorentzian contribution (FWHM) in the Voigt profile fit was evaluated to be 0.02 cm^{-1}. These Gaussian and Lorentzian contributions were implemented in the Voigt profiles used in simulations presented in Fig. 4. The lifetime of the complex could not be determined from this analysis due to an overlap between the $K_a' \leftarrow K_a'' = 0 \leftarrow 0$ and $1 \leftarrow 1$ transitions and overlap of transitions of different tunneling components.

The (101) ← (000) ***band***

Four bands involving the (101) vibrational state were observed. Three were observed near the (101) ← (000) vibrational band of H_2O monomer while the combination band involving (101) and the intermolecular in-plane N_2 bending mode was observed to higher frequency. The a-type subband is shown in blue in panel (a) of Fig. 5. A comparison between this subband and the same involving the (200) vibrational state (bottom panel of Fig. 4) reveals a higher spectral density of transitions and a larger spectral extension of this band. This is firstly due to the energy level structure and tunneling dynamics occurring within the complex. Indeed, there is an inversion of the VRT energy level ordering for $K_a' = 0$ between the (200) and (101) vibrational state, as discussed before and illustrated in Fig. 3. In the a-type subband of

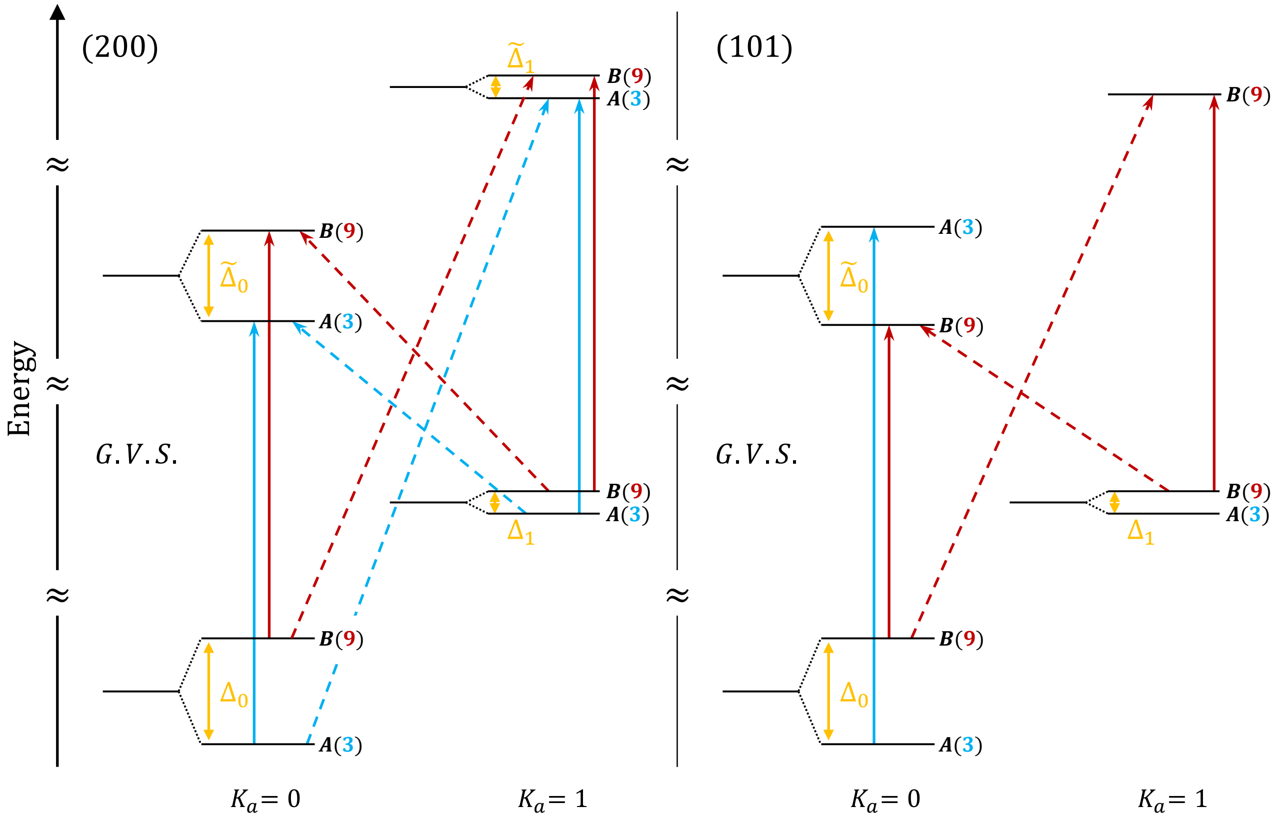

FIG. 3. Schematic representation of the vibration-rotation-tunneling energy levels of the N_2-H_2O complex, with their respective irreducible representation in G_8. The spin statistical weight are indicated in brackets. The values of the tunneling splitting in the ground vibrational state (*G.V.S.*) are from Ref. 4. Those for (200) vibrational state (left panel) and (101) vibrational state (right panel) are from this work. All the splittings are plotted on the same scale. The splitting associated with the water tunneling motion is noted as $\mathit{\Delta}_{K_a}$. The tilde character '$\sim$' indicates the splittings in the excited vibrational states. The vertical arrows represent the observed transitions from this work. Solid arrows represent *a*-type transitions and dashed arrows *b*-type transitions. The symbol '$\approx$' indicates a break in the vertical energy scale, which also applies to the vertical arrows. Due to the lack of information on the $K'_a = 1$, (101) *A* VRT state, this state is not shown on this figure.

TABLE II. N_2-H_2O molecular constants (in cm^{-1}) for the (200) vibrational excited state.

	Excited state (200)			
	A_1	A_2	B_1	B_2
ν_0	7200.51487(76)	7200.51623(82)	7200.11254(68)	7200.11673(68)
A	16.8893(12)	16.8345(18)	15.14418(91)	15.14433(91)
B	0.096779(27)	0.096664(45)	0.096408(20)	0.096411(20)
C	0.094716(26)	0.094758(45)	0.095418(23)	0.095375(23)
10^3D_{JK}	-3.070(23)	-3.335(42)	-2.334(15)	-2.335(15)
10^6D_J	1.677(46)	1.634(42)	1.610(99)	1.570(99)
10^6d_1	-0.336(53)	-0.66(14)	-0.082(31)	-0.122(31)
10^6H_{JK}	-0.636(81)	-0.37(19)	-0.860(51)	-0.871(51)
10^9H_J			-0.23(16)	0.21(16)

the $(101) \leftarrow (000)$, we observe the sum of the water tunneling splittings in the ground ($\mathit{\Delta}_0$) and excited ($\tilde{\mathit{\Delta}}_0$) vibrational states. The amplitude of this splitting in the ground vibrational state was predicted[4] to be 2.80 cm^{-1} and is expected to be smaller in the excited vibrational state, as it is the case in other vibrational excited states for this complex[5,11] and its isotopologue N_2-D_2O.[4,12] We therefore expected the origin of the *A* VRT state to lie about 5.6 cm^{-1} away from the origin of the *B* VRT state, which is indeed very close to the observed value of 5.44 cm^{-1}. Another difference between the $(200) \leftarrow (000)$ and $(101) \leftarrow (000)$ *a*-type subbands is the intensity and linewidth of the individual transitions. As is the case in the isolated H_2O, the $(101) \leftarrow (000)$ in N_2-H_2O is significantly more intense than the $(200) \leftarrow (000)$ band. Also, narrower transitions are observed for the $(101) \leftarrow (000)$ than

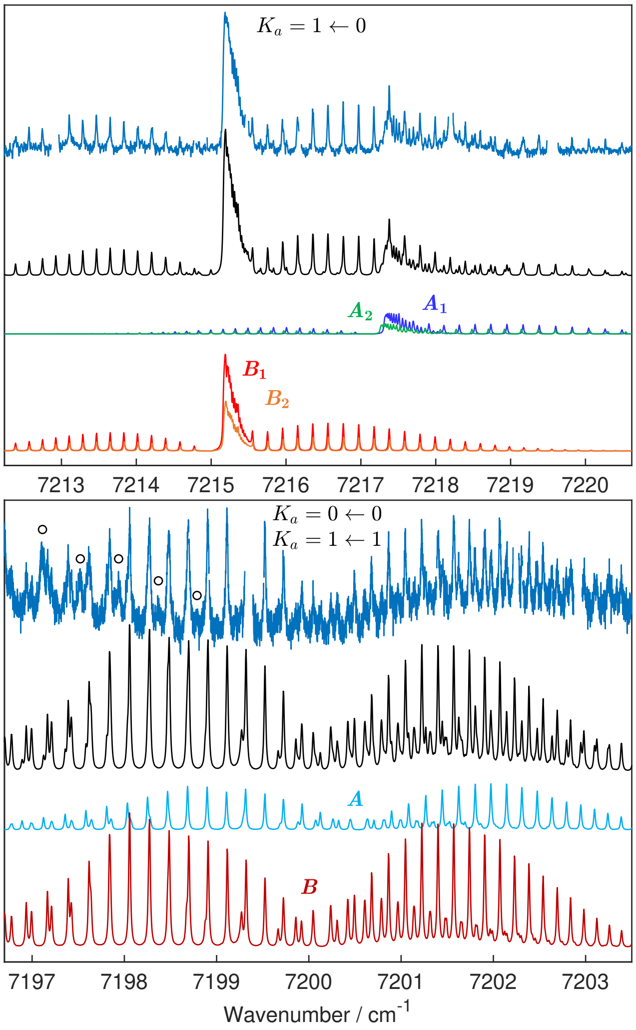

FIG. 4. Spectra of the $N_2 - H_2O$ complex in the (200) vibrational excited state region of H_2O. The upper panel shows the overtone b-type $K_a' \leftarrow K_a'' = 1 \leftarrow 0$ subband and the lower panel shows the a-type $K_a' \leftarrow K_a'' = 0 \leftarrow 0$ and $1 \leftarrow 1$ subbands. In each panel the observed spectrum is depicted in blue and the black trace is the sum of the simulated spectra of the different tunneling components. The unassigned broad lines on the left of the a-type subband marked with a black circle 'o' are due to the water dimer (see Ref. 28) and gaps in the observed spectra are regions of water monomer absorption.

for the $(200) \leftarrow (000)$ band. The Lorentzian contribution to the Voigt line profile in (101) was determined to be around 0.01 cm^{-1}. Again, the lifetime of the complex could not be determined. However, the narrower linewidth allows for the observation of the asymmetry doublets in the much weaker $K_a' \leftarrow K_a'' = 1 \leftarrow 1$ subband.

Several local perturbations were observed for transitions involving the $K_a' = 0$ and 1 states of $(101) \leftarrow (000)$ band, which made the rotational assignment somewhat challenging. Dashed rectangles in panel (a) of Fig. 5 show the perturbed regions in the $K_a' \leftarrow K_a'' = 0 \leftarrow 0$ subband.

To identify the perturbing state, a plot of the reduced energy for the B_1 (red) and B_2 (orange) VRT states as a function of J', reached by "pairs" of P (circles 'o') and R (asterisks '*') transitions was made. This is shown in panel (b) of Fig. 5. The reduced energy of a tunneling state was obtained using $E' - \bar{B}'J'(J'+1) + D_J'J'^2(J'+1)^2 - H_J'J'^3(J'+1)^3$, where E' is the excited state energy and the rotational constants taken from Table III, where $\bar{B}' = \frac{B'+C'}{2}$. As can be seen, an avoided crossing occurs between $J' = 11$ and 12 for the B_1 VRT state (in red). Subsequently, transitions belonging to the perturbing state were assigned. They are marked with purple dots in panel (a) of Fig. 5. The reduced energy of these states is also shown in purple in panel (b). They were calculated using the rotational and distortion constants of the B_1 (101) state from Table III. The avoided crossing plot indicates that the perturbing state has a lower vibrational origin and a larger $\bar{B}$ value. Thus, the most probable perturbing state is either (200) or a combination band involving (200) and an intermolecular mode. Considering the vibrational band origin of the B_1 VRT state, the perturbing state must lie below 7244.50 cm^{-1} (see Table III). Assuming a small inter/intra-molecular coupling one can combine the theoretical predictions made in the *G.V.S.*[4] with parameters for (200) vibrational state from this work to provide possible assignment of the perturbing state. Following this procedure, three candidates were found for the perturbing state (see Table II of Ref. 4):

1. The combination of the first intermolecular mode ν_{int1} added to the (200) vibrational excitation, with $K_a' = 0$ ($0_{0,0}$ energy level predicted at 7234.88 cm^{-1}).
2. The combination of the first intermolecular mode ν_{int1} added to the (200) vibrational excitation, with $K_a' = 1$ ($1_{1,1}$ energy level predicted at 7232.78 cm^{-1}).
3. The (200) vibrational excitation, with $K_a' = 2$ ($2_{2,0}$ energy level predicted at 7241.37 cm^{-1}).

The first and second candidates are most probably the $K_a' = 0$ and 1 states of the intermolecular N_2 in-plane bending mode, that we observed for $K_a' = 1$ in the $(101) \leftarrow (000)$ region. Eventhough we scanned the region between 7230 and 7240 cm^{-1}, we did not observe this band, likely due to its low intensity. From the band centers given above, it is unlikely that the perturbing state is either the first or the second candidate. There now remains the $K_a' = 2$ of the (200) vibrational state, for which the origin (energy of the $2_{2,0}$ rotational level) is predicted to be 7241.37 cm^{-1}. This value is just below the origin of the $K_a' = 0$ (101) B_1 state (7244.50 cm^{-1}), making it a good candidate for the perturbing state. As the perturbed rovibrational levels are e levels, the perturbing rovibrational levels must also be e levels. The e or f labeling is made following Ref. 29. This is also explained in the last section of the supplementary materials (the e levels of the asymmetry $K_a = 2$ doublets are the $J_{2,J-2}$ levels, i.e. $8_{2,6}$, $9_{2,7}$, $10_{2,8}$,...). Furthermore, since we observed the same perturbation for the B_2 VRT state in (101), we conclude that the perturbing state should have a small $N - N$ tunneling splitting. This is reasonable since the $N - N$ tunneling splitting for this state in the *G.V.S.* is predicted to be around 0.2 cm^{-1}.[4] Some of the perturbation allowed transitions were subsequently assigned.

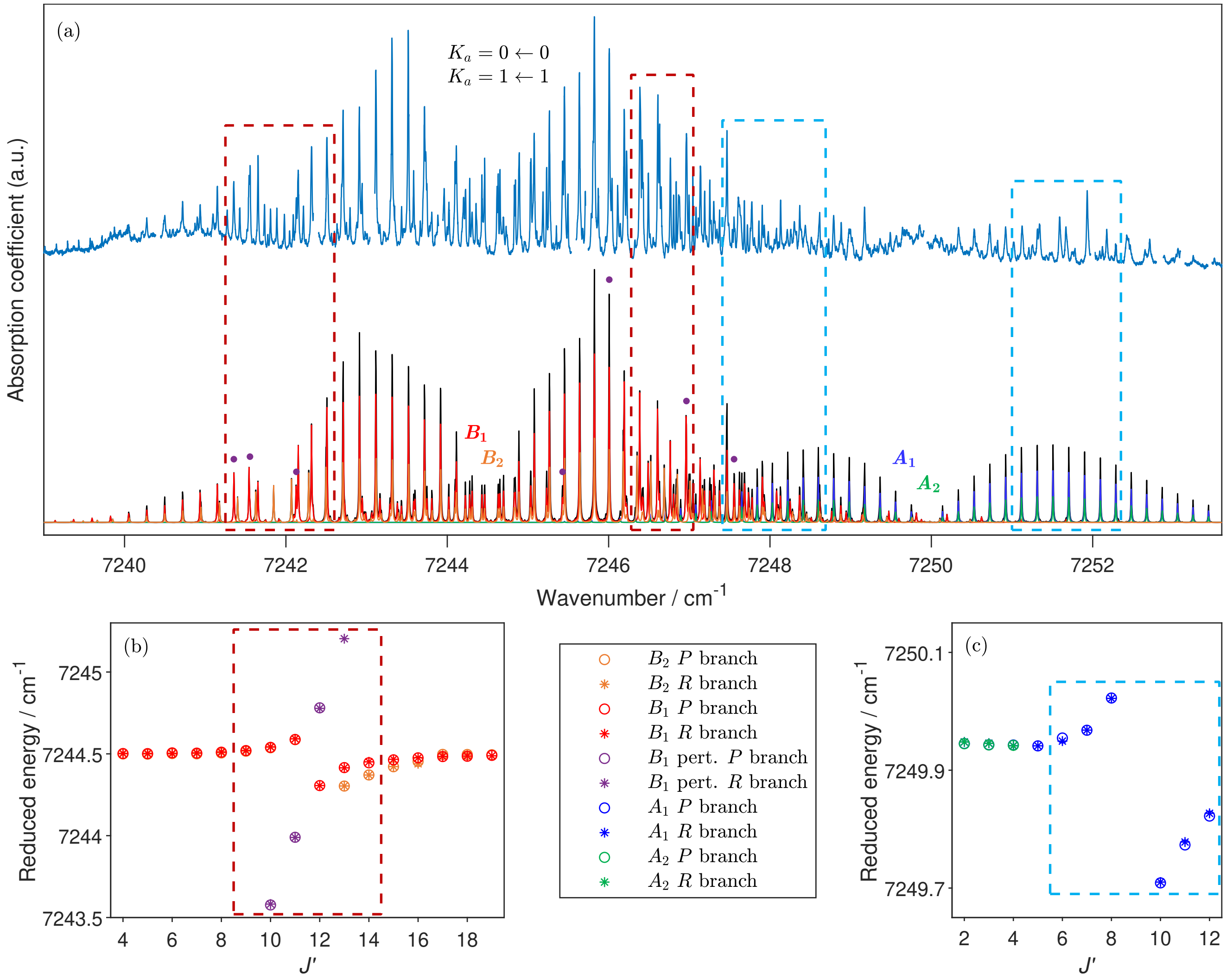

FIG. 5. Panel (a) shows the measured (top) and simulated (bottom) spectrum for the a-type $K_a' \leftarrow K_a'' = 0 \leftarrow 0$ and $1 \leftarrow 1$ subbands of the $N_2 - H_2O$ complex in the (101) state of H_2O. The underlying broad features around 7241 cm^{-1} and 7250 cm^{-1} are associated with $H_2O - H_2O$ (see Ref. 28). Gaps in the observed spectra are regions of water monomer absorption. The black trace is the sum of the simulated contribution from the B_1 (red), B_2 (orange), A_1 (dark blue) and A_2 (green) states. The dashed red (blue) rectangular areas are sections in which local perturbations were observed for the $K_a' = 0$ B (A) VRT states. Absorption lines marked with purple in the simulated spectrum indicate lines assigned to the perturbing state of B_1. Panel (b) / (c) illustrate respectively the reduced energy of the $K_a' = 0$ B_1 and B_2 / A_1 and A_2 VRT states as a function of the upper state J'. The avoided crossing regions in panel (b) and (c) correspond to the rectangular regions in panel (a).

The perturbation was satisfactorily modeled using the following matrix elements:

$$\langle(101),J,k|H|(200),J,k\pm2\rangle = \xi \times$$
$$\sqrt{[J(J+1)-(k\pm1)(k\pm2)]\times[J(J+1)-k(k\pm1)]},$$

where k is signed K_a and ξ is the Coriolis-type interaction parameter. The origin and distortion constants of the perturbing state were fixed to their values for the (200) state, only the A and $\bar{B}$ constants were fitted for this state. From the fit and assignment performed above, the origin (energy of the $2_{2,0}$ level) of the perturbing state was determined to be 7241.94 cm^{-1}. However, the A rotational constant has a much lower value than expected (10.40 cm^{-1} compared to 15.14 cm^{-1} for the $K_a' = 0$ and 1 states in the (200) vibrational state) and a $\bar{B}$ which is slightly larger. This is actually in a very good agreement with the values of $A = 10.26$ cm^{-1} and $\bar{B} = 0.1046$ cm^{-1} determined from the calculated values by Wang and Carrington Jr..[4] The surprising large change of A as a function of K_a can be associated with the non-rigidity of the complex and its value should be considered as an effective value.

For the A_1 and A_2 VRT states, only few transitions were assigned in the $K_a' \leftarrow K_a'' = 0 \leftarrow 0$ subband using the lower state combination differences. This is explained by the density of transitions and the local perturbation starting at $J' = 6$, highlighted by the light blue rectangle in panels (a) and (c) of Fig. 5. Panel (c) shows the reduced energy of the A_1 and A_2 states as a function of J'. Again, an avoided crossing is observed between $J' = 8$ and 10 ("pair" of P/R transitions associated with $J' = 9$ were not assigned) for the A_1 state. The perturbed transitions of the A_2 state were not assigned because of the weakness of the band. Due to the higher origin of the $K_a' = 0$ (101) A states compared with the B states (5.44 cm^{-1}), it is very unlikely that the perturbing state is the same for the A and B tunneling states. Indeed, the origin of the $K_a' = 2$ (200) A state (energy of the $2_{2,0}$ level) is predicted to be 7242.52 cm^{-1}, 7 cm^{-1} away from the origin of the $K_a = 0$ (101) A state (7249.94 cm^{-1}). A tentative assignment for the perturbing state is the second intermolecular mode ν_{int2} combined with (200), whose predicted origin equals 7251.81 and 7249.51 cm^{-1} for the $K_a' = 0$ and 1 ($1_{1,1}$ energy level) state, respectively.

Concerning the $K_a' \leftarrow K_a'' = 1 \leftarrow 0$ subband in (101), shown in the bottom panel of Fig. 6, only transitions for the B state were assigned. Indeed, only one intense Q-branch was observed. This was assigned to an overlap of the B_1 and B_2 VRT states. The P and R branches were first assigned and fitted using lower state combination differences, which led to the assignment of the Q transitions. This assignment is also supported by the observation of $K_a' \leftarrow K_a'' = 1 \leftarrow 1$ subband in $(101) \leftarrow (000)$. A perturbation was again observed for this subband, starting at $J' = 9$ and acting on the e levels of $K_a' = 1$ (101) B states, i.e $9_{1,9}, 10_{1,10}, \ldots$ as illustrated with asterisks '*' in the bottom panel of Fig. 6. Of course, the same perturbation was observed for this state in the $K_a' \leftarrow K_a'' = 1 \leftarrow 1$ subband. We were not able to treat the perturbation but only assigned "pairs" of P and R perturbed transitions using lower state combination differences. Those transitions were not included in the global fit. The origin of the perturbation will be discussed in the next section.

The b-type band in the top panel of Fig. 6 was assigned to the combination band of the (101) intramolecular vibration of H_2O and the intermolecular N_2 in-plane bending vibration, as discussed in Sec. IV. As can be seen in Fig. 6, only the subbands belonging to the B state were assigned. The assignment of the B_1 subband was performed in the same way as the b-type subbands of (101), but here the observed local perturbation affects the low J values of the e levels marked with asterisk '*'. The assignment of the B_2 subband was complicated by perturbations and the limited laser coverage available at the higher frequency side. Hence, no unperturbed "pairs" of P/R transitions could be assigned. Due to pile up of the transitions near the band center, the assignment of the Q-branch is uncertain by unity in the value of J. The assignment for the B_2 tunneling subband was not included in the global fit and a separate fit was performed. The fitted parameters are given in Table III. As we only had access to the $K_a' = 1$ states for this band, the A rotational constant could not be computed and was fixed to its value in the (101) vibrational excited state of the B_1 and B_2 VRT states.

All the rotational constants from the fit and discussion above in the $(101) \leftarrow (000)$ region of water are given in Table III. The assigned transitions can be found in Tables S-5 to S-7 of the supplementary materials.

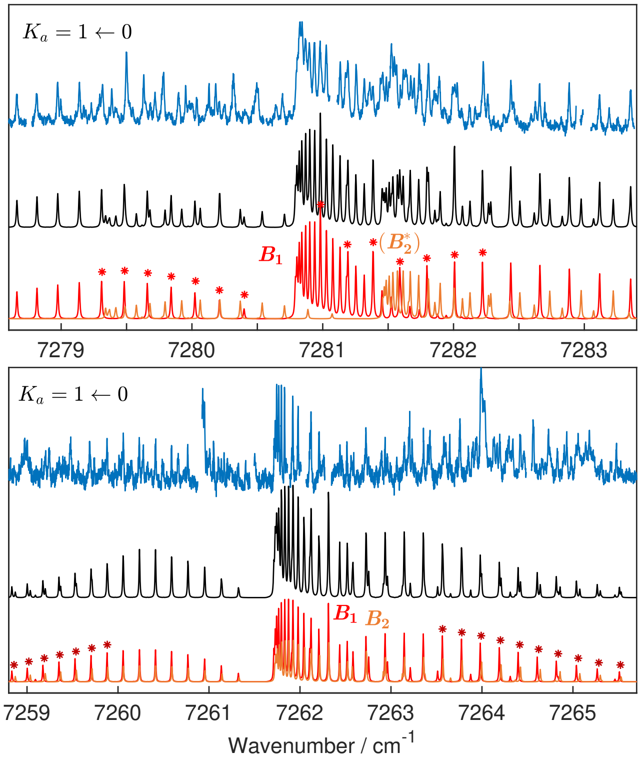

FIG. 6. Spectra of the $N_2 - H_2O$ complex in the (101) vibrational excited state region of H_2O. The upper panel shows the b-type $K_a' \leftarrow K_a'' = 1 \leftarrow 0$ combination band involving the in-plane N_2 bending intermolecular mode and the lower panel shows the b-type $K_a' \leftarrow K_a'' = 1 \leftarrow 0$ (101) overtone band. In each panel the observed spectrum is depicted in blue and the black trace is the sum of the simulated spectra of the different tunneling components. Perturbed lines are marked with an asterisk '*'. The assignment for the Q-branch of the B_2 subband in the top panel is tentative.

IV. DISCUSSION

A. The $(101) + \nu_{int} \leftarrow (000)$ band assignment

The assignment of the band around 7281 cm^{-1} to the combined excitation of the intermolecular in-plane N_2 bending mode and of the intramolecular (101) vibration of H_2O was not straightforward due to the proximity with both the (200) and (101) vibrational origins. Indeed, the origin of this band is located 37 and 81 cm^{-1} away from the band origins of (101) and (200), respectively. For a combination with (200) the most probable intermolecular modes are the stretch, the in-plane N_2 bend or the out-of-plane N_2 bend. Ellington *et al.*[7] evaluated these to be at 86, 43 and 53 cm^{-1}, respectively. More precise predictions, leading to the same conclusions, were provided by Wang and Carrington Jr[4] and Wang *et al.*[5] but without the vibrational assignment. Considering the large A rotational constant of this complex and that this b-type combination band involves a $K_a' = 1$ value, one can rule out the van der Waals stretch and the out-of-plane N_2 bending modes. Another possibility is the combination of (200) with the double excitation of the in-plane N_2 bending motion. This

TABLE III. $N_2 - H_2O$ molecular constants (in cm^{-1}) [a] for the (101) and $(101) + \nu_{int}$ vibrational excited states. The rotational constants of the fitted perturbing state (B_1^* state) arising from the (200) vibrational excited state are also given.

	Excited state (101)					$(101) + \nu_{int}$	
	A_1	A_2	B_1	Perturbing state* (200) $K_a = 2$ B_1	B_2	B_1	(B_2^*)
ν_0	7249.9446(21)	7249.9488(26)	7244.50290(65)	7200.11254 [b]	7244.50409(96)	7263.5831(16)	7264.2437(41)
A	16.8893 [c]	16.8345 [c]	17.30226(96)	10.4016(16) [d]	17.3101(13)	17.30226 [e]	17.3101 [e]
B			0.097660(46)		0.097958(61)	0.100780(31)	
C			0.095293(48)		0.095426(60)	0.097639(36)	
$\bar{B}$	0.09737(15)	0.09696(19)		0.108569(47)			0.099710(62)
$10^3 D_{JK}$			-3.037(37)	-2.334 [f]	-2.566(52)		
$10^6 D_J$	3.22(84)		1.824(87)	1.610 [f]	4.63(17)	0.917(84)	-5.14(18)
$10^6 d_1$			3.27(30)	-0.082 [f]	2.70(35)	-1.696(57)	
$10^6 H_{JK}$			-2.84(36)	-0.860 [f]	2.95(42)		
$10^9 H_J$	2.8(12)		0.84(13)	-0.23 [f]	5.33(24)		
$10^9 L_{JJK}$			12.16(39)				
ξ			$-0.0010736(41)$				

[a] Numbers in parentheses are the uncertainties and are in the same units.
[b] The origin of this state was fixed to the origin of the (200) vibrational excited state during the fit.
[c] The *A* rotational constant was fixed to its (200) vibrational excited state value during the fit.
[d] This surprising value of the *A* rotational constant can be associated to the non-rigidity of the complex (see main text).
[e] The *A* rotational constant was fixed to its (101) vibrational excited state value during the fit.
[f] The values of the distortion constants were fixed to the ones of the (200) vibrational excited state during the fit.

can also be ruled out due to the fact that we have not been able to observe any combination bands involving (200) state.

Finally, as the $(101) \leftarrow (000)$ is much stronger than the $(200) \leftarrow (000)$ and based on the intensity ratio found in this work between the intramolecular excitation (101) and the combination band, that is similar to the one observed in $N_2 - D_2O$ in the OD asymmetric stretch region,[12] the band was assigned to the combined excitation of the intermolecular in-plane N_2 bending mode and of the intramolecular (101) vibration of H_2O.

B. Perturbations

Several local perturbations were observed in the (101) region. These affect the $K_a' = 0$, $K_a' = 1$ of (101) and $K_a' = 1$ of $(101) + \nu_{int}$ states. Only in the case of $K_a' = 0$ (101) for the B_1 VRT state, were we able to assign and fit the perturbing state and retrieve rotational constants as detailed in Sec. III.

All the observed perturbations act locally on the rovibrational energy levels of the complex indicating Coriolis couplings. Considering the dissociation limit of the complex (245 cm^{-1})[3,4], that the perturbations do not affect the observed linewidth and the density of vibrational states, the perturbing state has to be (200) or a combination of intermolecular mode(s) with (200). We also note that all the perturbed levels have *e* symmetry.

Perturbation of $K_a' = 1$ *of* (101)

Perturbations were observed for $K_a' = 1$ B_1 and B_2 VRT states of (101) for the same set of J' values (see bottom panel of Fig. 6). From the assignment of some perturbed P/R "pairs" of transitions, reaching the same upper state (see Sec. III), an avoided crossing was observed around $J' = 9$. From the shape of this avoided crossing, the perturbing state was found to have a higher vibrational origin and a lower $\bar{B}$ rotational constant compared to those of (101). Since the perturbation acts on both B_1 and B_2 for the same J' values, we conclude that the $N - N$ tunneling splitting must be similarly small for the perturbing state. Also, because the perturbation is only observed for the *e* levels, it is unlikely that the perturbing state is a $K_a' \geq 2$ level as the asymmetry doublets for $K_a' \geq 2$ values are expected to be small (~ 0.005 cm^{-1}). Further support for this comes from the absence of perturbations observed in the *Q*-branch which involves the *f* levels. Considering theoretical predictions in the *G.V.S.* from Ref. 30 and assuming small inter-intramolecular couplings, the closest perturbing state is the $K_a' = 1$ state of $(200) + \nu_{int3}$ whose origins are located at 7263.64 cm^{-1} and 7270.37 cm^{-1} for B_1 and B_2, respectively. But this mode is predicted to have a very large $N - N$ tunneling splitting which makes it an unlikely candidate for a perturbing state. Another and more realistic candidate is the $K_a' = 0$ $(200) + \nu_{int5}$ state whose predicted origins are 7264.88 and 7264.83 cm^{-1} for both B_1 and B_2 states, indicating first a small $N - N$ tunneling splitting and an origin located higher than the $K_a' = 1$ (101) states, as required. Furthermore, the calculated $\bar{B}$ rotational constant is equal to 0.0929 and 0.0922 cm^{-1} for the B_1 and B_2 states, respectively.[30] These values are also lower than the $\bar{B}$ for the (101) vibrational excited state given in Table III. The discussion above suggests the perturbation observed in the $K_a' = 1$ B_1 and B_2 tunneling states of (101) states is likely due to the $K_a' = 0$ $(200) + \nu_{int5}$ state.

Perturbation of $K_a' = 1$ *of* $(101) + \nu_{int}$

Several "pairs" of P/R transitions are also perturbed in the case of $K_a' = 1$ of $(101) + \nu_{int}$ as marked with asterisks in the top panel of Fig. 6. The inspection of the avoided crossing region and the direction of the perturbation indicates that the perturbing state has a smaller $\bar{B}$ rotational constant as well as a higher (ro)vibrational origin. Being 80 cm^{-1} above the origin of the (200) vibrational origin, the number of possible states is too large to reach a sound or even a tentative assignment for the perturbing state.

A general comment concerning the perturbations around (101) *in water containing hetero-dimers*

For $\mathrm{N_2-H_2O}$, the subbands observed around (200) are well behaved in terms of position and intensity, in contrast to the (101) subbands where every K_a' stack of states is perturbed due to the proximity to combination states involving (200). This is also the case in other water containing complexes such as $\mathrm{CO_2-H_2O}$[31] and $\mathrm{Ar-H_2O}$.[32] A similar behaviour was also observed in the mid-Infrared in the case of $\mathrm{N_2-D_2O}$ for (100) and (001).[12]

C. Evolution of the intermolecular dynamics with the intramolecular excitation

For $\mathrm{N_2-H_2O}$, one can qualitatively track the coupling between intra- and inter-molecular degrees of freedom with the intramolecular excitation using different observables, i.e. the vibrational shift, the tunneling splitting and the intermolecular frequency retrieved from the observation of a combination band. In this section, we review the results from this work and previous studies to draw conclusions on how this coupling evolves as a function of the intramolecular excitation, with intramolecular vibrational excitation up to 29 times the dissociation energy.

Vibrational shifts

The band-origins of the (200) and (101) states of the complex were computed by averaging the vibrational band-origins of tunneling components given in Tables II and III and are equal to 7200.315 and 7247.225 cm^{-1}, respectively. The calculated band origins are redshifted by 1.225 cm^{-1} and 2.592 cm^{-1} from that of the $\mathrm{H_2O}$ monomer.[24,25] Table IV gives the shifts for the $\mathrm{N_2-D_2O}$, $\mathrm{N_2-H_2O}$ and $\mathrm{CO_2-H_2O}$ complexes for different vibrational states. The vibrational shifts of the $\mathrm{N_2-H_2O}$ complex were computed using Refs. 11, 33 and this work, those for $\mathrm{N_2-D_2O}$ and $\mathrm{CO_2-H_2O}$ were taken from Refs. 12, 20, 24, 25, 31, 34–36.

TABLE IV. Vibrational shifts (in cm^{-1}) of the $\mathrm{N_2-D_2O}$, $\mathrm{N_2-H_2O}$ and $\mathrm{CO_2-H_2O}$ complexes. Negative (positive) values indicate a redshift (blueshift) of the band origin of the complex compared to the one of the water monomer.

	(010)	(100)	(001)	(200)	(101)
$\mathrm{N_2-H_2O}$ [a]	2.261			−1.225	−2.592
$\mathrm{N_2-D_2O}$ [b]	1.247	−0.629	−1.811		
$\mathrm{CO_2-H_2O}$ [c]	0.739		−3.020	−3	−6.1

[a] Computed using Refs. 11, 24, and 25 and this work.
[b] From Refs. 12, 33, and 34.
[c] From Refs. 20, 31, 35, and 36.

From Table IV, there is a clear trend for the shift as a function of excitation of the intramolecular degrees of freedom in the water entity. The bending (010) excitation of water has a blueshift whereas the symmetric (100) and asymmetric (001) stretch excitations experience redshifts, with a larger shift for the excitation of the asymmetric stretch.

Larger shifts of around -2, -17 and -26 cm^{-1} have been observed for the (010), (100) and (001) fundamental vibrations of the complex.[13–17] Nevertheless, these results were obtained for $\mathrm{H_2O}$ and $\mathrm{N_2}$ embedded in Ar/Kr matrices. An additional He droplets study gives redshifts values of around -5 cm^{-1} for both (100) and (001) intramolecular $\mathrm{H_2O}$ excitation in $\mathrm{N_2-H_2O}$.[18] Those values are not directly comparable to the values determined for the isolated complex, as outlined in different studies (cfr.[37] for example).

Vibrational depedency of the tunneling splitting

From rotationally resolved spectra we can only have access to the sum (or difference) of the tunneling splittings between the ground and excited vibrational states. An averaged sum or difference for the $K_a' = 0$ and $K_a' = 1$ tunneling splittings in the excited vibrational state can also be found using the measured vibrational origin ν_0 and the A and $\bar{B}$ rotational constants of each tunneling component. From the left panel of Fig. 3, we measure the difference between the water tunneling splittings in the ground and excited vibrational state of (200) for $K_a = 0$. This can be found using ${}^rR^A_{0,1}(0) - {}^rR^B_{0,1}(0) = \Delta_0(0) - \tilde{\Delta}_0^{(200)}(1)$. The superscript on Δ indicates the corresponding vibrational excited state. On the other hand, by referring to the right panel of Fig. 3, we measure the sum of the water tunneling splittings in the ground and excited vibrational state of (101) for $K_a = 0$ given by ${}^rR^A_{0,1}(0) - {}^rR^B_{0,1}(0) = \Delta_0(0) + \tilde{\Delta}_0^{(101)}(1)$. Since we are interested in the vibrational dependency of the tunneling splitting, we will use the calculated *G.V.S.* values of the tunneling splittings by Wang and Carrington Jr[4] ($\Delta_0(0) = 2.7998$ cm^{-1}) and the rotational constants obtained from our global fit given in Tables II, III and S-1 to calculate the tunneling splittings in the excited vibrational states. The K_a dependency of the water tunneling splitting is also investigated when possible. Table V gives the calculated values of the water tunneling splitting for $K_a = 0$ or 1 in the *G.V.S.*, (010), (200) and (101) vibrational states.

TABLE V. Calculated water tunneling splittings in $N_2 - H_2O$ (in cm^{-1}) for the ground (*G.V.S.*) and (010), (200), (101) vibrational states (from Refs. 4, 10, and 34 and this work).

	G.V.S.	(010)	(200)	(101)
$\Delta_0(0)$	2.7998 [a]			
$\tilde{\Delta}_0(0)$		2.4131	2.3989	2.6434
$\Delta_1(1)$	0.7006 [b]			
$\tilde{\Delta}_1(1)$		1.0099	0.6813	

[a] From Ref. 4.

[b] Computed with Ref. 4 and transitions from Ref. 10 (refined constants in Table I).

As can be seen from Table V, the water tunneling splitting depends strongly on K_a, with an amplitude decreasing by a factor of 2 or more in $K_a = 1$ compared to $K_a = 0$. Interestingly the tunneling splitting for $K_a = 0$ has a much weaker dependence on the intramolecular vibrational excitation.

Intermolecular vibration

The difference between the origins of $(101) + \nu_{int}$ and (101) provides an intermolecular frequency of 36.48 (B_1) and around 37.15 cm^{-1} (B_2) for the in-plane bending mode of the N_2 entity within the complex. These values are within ~ 10 % of the calculated ones[4] determined for the G.V.S, 32.66 (B_1) and 32.73 cm^{-1} (B_2). The agreement with *G.V.S.* calculations[4] was on the order of 2 % in our previous study of $N_2 - D_2O$ performed in the 1OD region.[12] The 10 % difference is associated with approximations performed in the theoretical study and change of the intermolecular frequencies following the intramolecular OH excitation. The relative weight of these two contributions cannot be determined at this stage. Further advanced calculations as the ones performed recently for $H_2O - H_2O$[38] could probably tackle this.

V. CONCLUSION AND PERSPECTIVES

The first overtone spectral signatures and analyses of the $N_2 - H_2O$ complex in the 2OH stretch region were presented in this work. The rovibrational assignment was made by considering the tunneling motions occurring inside the complex due to its four equivalent versions. Several perturbations were highlighted in the (101) region and one of them was modeled through an effective Coriolis coupling with the $K_a' = 2$ (200) state. The water tunneling splitting was found to depend slightly on the vibrational excited state and strongly on the K_a value. Vibrational shifts due to the complexation were retrieved and compared with other water containing van der Waals complexes. The assignment performed in this work is a step forward for the characterization of the PES of this important complex.

ACKNOWLEDGMENTS

The authors would like to thank X.-G. Wang and T. Carrington Jr. for sharing their results. The ULB and SQUARES service are warmly acknowledged for the loan of the FANTASIO+ set-up. This work was funded by the Action de Recherches Concertées (Grant No. ARC iBEAM-18/23-090) and the FNRS CDR J.0113.23 and J.0129.20. R.G. is a FRIA grantee of the Fonds de la Recherche Scientifique (FNRS).

DATA AVAILABILITY

The data that support the findings of this study are either available from the supplementary materials or from the corresponding author upon reasonable request.

REFERENCES

[1] H. G. Kjaergaard, T. W. Robinson, D. L. Howard, J. S. Daniel, J. E. Headrick, and V. Vaida, J. Phys. Chem. A **107**, 10680–10686 (2003).

[2] Y. Kasai, E. Dupuy, R. Saito, K. Hashimoto, A. Sabu, S. Kondo, Y. Sumiyoshi, and Y. Endo, Atmos. Chem. Phys. **11**, 8607–8612 (2011).

[3] A. S. Tulegenov, R. J. Wheatley, M. P. Hodges, and A. H. Harvey, J. Chem. Phys. **126**, 094305 (2007).

[4] X.-G. Wang and T. Carrington Jr, J. Chem. Phys. **143**, 024303 (2015).

[5] L. Wang, X.-L. Zhang, Y. Zhai, M. Nooijen, and H. Li, J. Chem. Phys. **153**, 054303 (2020).

[6] J. Sadlej, B. Rowland, J. P. Devlin, and V. Buch, J. Chem. Phys. **102**, 4804–4818 (1995).

[7] T. L. Ellington and G. S. Tschumper, Comput. Theoret. Chem. **1021**, 109–113 (2013).

[8] H. G. Kjaergaard, G. R. Low, T. W. Robinson, and D. L. Howard, J. Phys. Chem. A **106**, 8955–8962 (2002).

[9] H. O. Leung, M. D. Marshall, R. D. Suenram, and F. J. Lovas, J. Chem. Phys. **90**, 700–712 (1989).

[10] P. A. Stockman, *Microwave and far-infrared spectroscopy of water-containing, hydrogen-bonded dimers: vibrational, rotational, and tunneling dynamics*, Ph.D. thesis, California Institute of Technology (1996).

[11] S. Springer, B. McElmurry, Z. Wang, I. Leonov, R. Lucchese, J. Bevan, and L. Coudert, Chem. Phys. Let. **633**, 229–233 (2015).

[12] R. Glorieux, C. Lauzin, A. J. Barclay, M. Herman, and N. Moazzen-Ahmadi, J. Chem. Phys. **155**, 174309 (2021).

[13] L. Andrews and S. R. Davis, J. Chem. Phys. **83**, 4983–4989 (1985).

[14] A. Engdahl and B. Nelander, J. Mol. Struct. **193**, 101–109 (1989).

[15] S. Coussan, A. Loutellier, J. Perchard, S. Racine, and Y. Bouteiller, J. Mol. Struct. **471**, 37–47 (1998).

[16] S. Hirabayashi, K. Ohno, H. Abe, and K. M. Yamada, J. Chem. Phys. **122**, 194506 (2005).

[17] C. Pardanaud, A.-M. Vasserot, X. Michaut, and L. Abouaf-Marguin, J. Mol. Struct. **873**, 181–190 (2008).

[18] S. Kuma, M. N. Slipchenko, K. E. Kuyanov, T. Momose, and A. F. Vilesov, J. Phys. Chem. A **110**, 10046–10052 (2006).

[19] K. Didriche, , C. Lauzin, T. Földes, X. de Ghellinck D'Elseghem Vaernewijck, and M. Herman, Mol. Phys. **108**, 2155–2163 (2010).

[20] A. S. Bogomolov, A. Roucou, R. Bejjani, M. Herman, N. Moazzen-Ahmadi, and C. Lauzin, Chem. Phys. Let. **774**, 138606 (2021).

[21] I. E. Gordon, L. S. Rothman, R. J. Hargreaves, R. Hashemi, E. V. Karlovets, F. M. Skinner, E. K. Conway, C. Hill, R. V. Kochanov, Y. Tan, P. Wcisło,

A. A. Finenko, K. Nelson, P. F. Bernath, M. Birk, V. Boudon, A. Campargue, K. V. Chance, A. Coustenis, B. J. Drouin, J.-M. Flaud, R. R. Gamache, J. T. Hodges, D. Jacquemart, E. J. Mlawer, A. V. Nikitin, V. I. Perevalov, M. Rotger, J. Tennyson, G. C. Toon, H. Tran, V. G. Tyuterev, E. M. Adkins, A. Baker, A. Barbe, E. Canè, A. G. Császár, A. Dudaryonok, O. Egorov, A. J. Fleisher, H. Fleurbaey, A. Foltynowicz, T. Furtenbacher, J. J. Harrison, J. Hartmann, V. Horneman, X. Huang, T. Karman, J. Karns, S. Kassi, I. Kleiner, V. Kofman, F. Kwabia–Tchana, N. N. Lavrentieva, T. J. Lee, D. A. Long, A. A. Lukashevskaya, O. M. Lyulin, V. Y. Makhnev, W. Matt, S. T. Massie, M. Melosso, S. N. Mikhailenko, D. Mondelain, H. S. P. Müller, O. V. Naumenko, A. Perrin, O. L. Polyansky, E. Raddaoui, P. L. Raston, Z. D. Reed, M. Rey, C. Richard, R. Tóbiás, I. Sadiek, D. W. Schwenke, E. Starikova, K. Sung, F. Tamassia, S. A. Tashkun, J. Vander Auwera, I. A. Vasilenko, A. A. Vigasin, G. L. Villanueva, B. Vispoel, G. Wagner, A. Yachmenev, and S. N. Yurchenko, "The HITRAN2020 molecular spectroscopic database," J. Quant. Spectrosc. Radiat. Transfer **277**, 107949 (2022).

[22] P. R. Bunker and P. Jensen, *Molecular symmetry and spectroscopy*, e-book ed. (NRC Research Press, Ottawa, Ontario, Canada, 2012) 748 p.

[23] L. Coudert and J. Hougen, J. Mol. Spec. **130**, 86–119 (1988).

[24] R. A. Toth, J. Quant. Spectrosc. Radiat. Transfer **94**, 51–107 (2005).

[25] J. Tennyson, P. F. Bernath, L. R. Brown, A. Campargue, A. G. Császár, L. Daumont, R. R. Gamache, J. T. Hodges, O. V. Naumenko, O. L. Polyansky, L. S. Rothman, A. C. Vandaele, N. F. Zobov, A. R. Al Derzi, C. Fábri, A. Z. Fazliev, T. Furtenbacher, I. E. Gordon, L. Lodi, and I. I. Mizus, J. Quant. Spectrosc. Radiat. Transfer **117**, 29–58 (2013).

[26] C. M. Western, "Pgopher: A program for simulating rotational, vibrational and electronic spectra," J. Quant. Spectrosc. Radiat. Transfer **186**, 221–242 (2017).

[27] J. K. G. Watson, J. Chem. Phys. **46**, 1935–1949 (1967).

[28] N. Suas-David, T. Vanfleteren, T. Földes, S. Kassi, R. Georges, and M. Herman, J. Phys. Chem. A **119**, 10022–10034 (2015).

[29] J. M. Brown, J. T. Hougen, K.-P. Huber, J. W. C. Johns, I. Kopp, H. Lefebvre-Brion, A. J. Mere, D. A. Ramsay, J. Rostas, and R. N. Zare, J. Mol. Spec. **55**, 500–503 (1975).

[30] X.-G. Wang and T. Carrington Jr., private communication (2022).

[31] C. Lauzin, A. C. Imbreckx, T. Földes, T. Vanfleteren, N. Moazzen-Ahmadi, and M. Herman, Mol. Phys. **118**, e1706776 (2020).

[32] T. Vanfleteren, T. Földes, M. Herman, J. Liévin, J. Loreau, and L. H. Coudert, J. Chem. Phys. **147**, 014302 (2017).

[33] J. Tennyson, P. F. Bernath, L. R. Brown, A. Campargue, A. G. Császár, L. Daumont, R. R. Gamache, J. T. Hodges, O. V. Naumenko, O. L. Polyansky, *et al.*, J. Quant. Spectrosc. Radiat. Transfer **142**, 93–108 (2014).

[34] Y. Zhu, R. Zheng, S. Li, Y. Yang, and C. Duan, J. Chem. Phys. **139**, 214309 (2013).

[35] Y. Zhu, S. Li, P. Sun, and C. Duan, J. Mol. Spec. **283**, 7–9 (2013).

[36] P. A. Block, M. D. Marshall, L. G. Pedersen, and R. E. Miller, J. Chem. Phys. **96**, 7321 (1992).

[37] S. Oswald, M. Wallrabe, and M. A. Suhm, J. Phys. Chem. A **121**, 3411–3422 (2017).

[38] X.-G. Wang and T. Carrington Jr, J. Chem. Phys. **158**, 084107 (2023).